Appl. Phys. A (2016) 122:927
DOI 10.1007/s00339-016-0458-0

Applied Physics A
Materials Science & Processing

A 2-DOF microstructure-dependent model for the coupled torsion/bending instability of rotational nanoscanner

M. Keivani[1] · N. Abadian[2] · A. Koochi[3] · J. Mokhtari[2] · M. Abadyan[3]

Received: 4 January 2016 / Accepted: 26 September 2016 / Published online: 3 October 2016

Abstract It has been well established that the physical performance of nanodevices might be affected by the microstructure. Herein, a two-degree-of-freedom model base on the modified couple stress theory is developed to incorporate the impact of microstructure in the torsion/bending coupled instability of rotational nanoscanner. Effect of microstructure dependency on the instability parameters is determined as a function of the microstructure parameter, bending/torsion coupling ratio, van der Waals force parameter and geometrical dimensions. It is found that the bending/torsion coupling substantially affects the stable behavior of the scanners especially those with long rotational beam elements. Impact of microstructure on instability voltage of the nanoscanner depends on coupling ratio and the conquering bending mode over torsion mode. This effect is more highlighted for higher values of coupling ratio. Depending on the geometry and material characteristics, the presented model is able to simulate both hardening behavior (due to microstructure) and softening behavior (due to torsion/bending coupling) of the nanoscanners.

✉ M. Abadyan
abadyan@yahoo.com

[1] Shahrekord University of Medical Sciences, Shahrekord, Iran

[2] Department of Mathematics, Isfahan (Khorasgan) Branch, Islamic Azad University, Isfahan, Iran

[3] Shahrekord Branch, Islamic Azad University, Shahrekord, Iran

1 Introduction

Ultra-small electrostatic torsional scanners due to the high sensitivity, high quality factor, low actuation voltage and small possibility of stiction have wide applications in the nanoelectromechanical systems (NEMS) and micro-opto-electro-mechanical systems (MOEMS), such as tunable torsional capacitors, digital light processing chips and torsional radio frequency switches used in microsatellites, communication instruments and radar systems [1–5]. Among these systems, torsional NEMS scanners are being considered as potential ultra-small devices with promising applications in fabrication of smart structures such as confocal microscopy, wireless communications, optical telecommunication, bar code reading, laser printing and endoscopic bio-imaging, integrated circuits, switching devices, nanorobots. Therefore, many researchers have focused on the numerical, theoretical and experimental analysis of such systems through different assumptions and methods [6–14]. Figure 1 shows the schematic of a typical rotational micro-/nanoscanner that is constructed from a movable mirror suspended above fixed conductive ground electrode. The movable component is a main plate (mirror) attached to two supporting rotational beams. The fixed component is a conductive exciting electrode which is fixed above a substrate. By imposing a DC voltage differential between the components, the main plane deflects and rotates, simultaneously. At a critical voltage, i.e., the pull-in voltage, the Coulomb torque/force exceeds the elastic resistance and the mirror adheres the fixed plane. Predicting the pull-in threshold is crucial for design and fabrication of the torsional scanners. In this regard, many investigators have focused on modeling the instability and determining the pull-in parameters of rotational systems [15–17]. Previous researchers have developed one-degree-

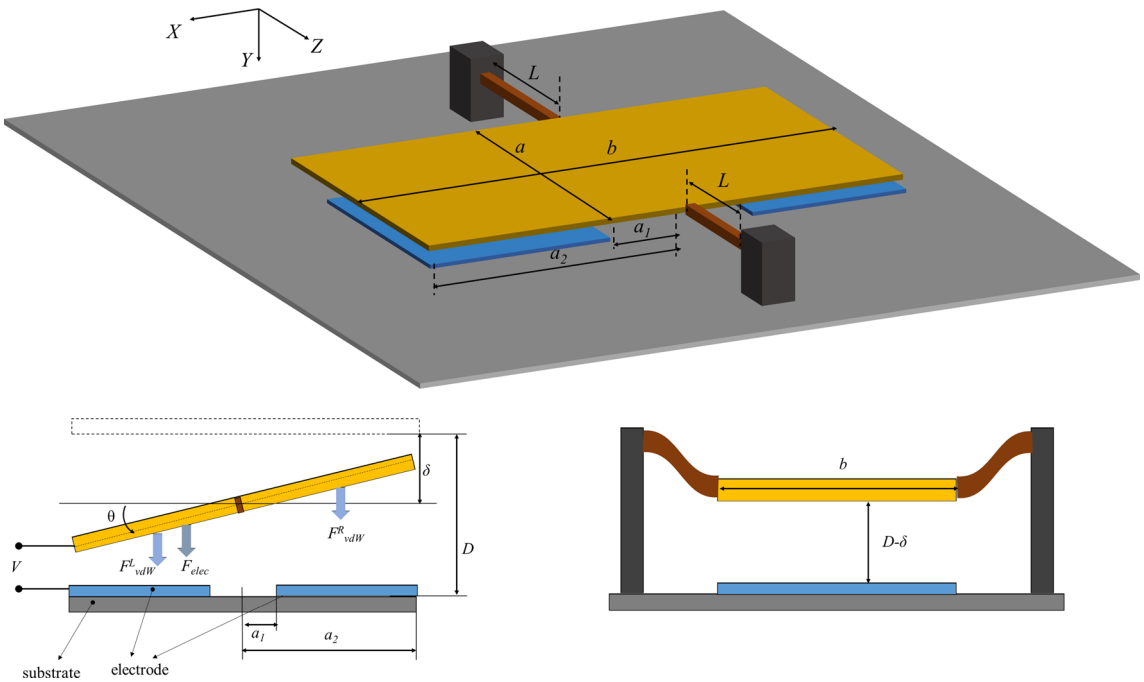

Fig. 1 Schematic diagram of rotational nanoscanner

of-freedom (1-DOF) models to capture the instability behavior of rotational mirrors [18–20]. The 1-DOF model has incorporated only the torsional instability mode and thus is reliable only if the deflection of the mirror is negligible. However, when the torsional-induced displacement and vertical deflection of the mirror are of the same order, the pull-in parameters could not be accurately computed via 1-DOF models. In this case, bending of the supporting beams should be taken into account as well as torsion. In this regard, other investigators have employed 2-DOF models to calculate the coupling between the bending and torsion instability of the rotational system [21–25]. This coupling can be considered in the coupled displacements or angles in total [26].

The scale dependency of material properties at small scale is an important phenomenon that might be crucial in ultra-small systems. If the characteristic dimension of metallic components be of the order of the intrinsic material length scale, a hardening trend in the mechanical characteristics of the components appears. Fleck et al. [27] have been observed the microstructure-dependent response of some materials in torsional loading. Therefore, the microstructure is considered as an important phenomenon that might affect the stable behavior of rotational scanners. This microstructure dependency of material characteristics of nanobeams can be modeled using size-dependent theories such as modified couple stress theory (MCST). This theory has been used by previous investigators in modeling the mechanical performance of microstructures [28–30]. In recent years, MCST has been employed for modeling the microstructure-dependent stability of electromechanically actuated beams and plates [31].

To the best knowledge of the authors, none of the previous researchers has incorporated the influence of microstructure in 2-DOF models used for simulating the rotational nano-/microscanners. Therefore, the authors present a new microstructure-dependent two-degree-of-freedom (2-DOF) model to incorporate the size phenomena in the torsion/bending coupled instability of rotational NEMS scanner. Since the van der Waals (vdW) force can highly affect the stability threshold of rotational systems [24, 32, 33], the vdW force is incorporated in the governing equation.

2 Fundamentals of MCST

Using the MCST, the strain energy U in region Ω is shown [34]

$$U = \frac{1}{2}\int_{\Omega}\left(\sigma_{ij}\varepsilon_{ij} + m_{ij}\chi_{ij}\right)\mathrm{d}V \tag{1}$$

where the stress tensor σ_{ij}, strain tensor ε_{ij}, deviatoric part of the couple stress tensor m_{ij} and symmetric curvature tensor χ_{ij} are defined by

$$\sigma_{ij} = \lambda tr(\varepsilon_{ij})I + 2\mu\varepsilon_{ij} \tag{2a}$$

$$\varepsilon_{ij} = \frac{1}{2}\left((\nabla u)_i + (\nabla u)_i^T\right) \tag{2b}$$

$$m_{ij} = 2l^2\mu\chi_{ij} \tag{2c}$$

$$\chi_{ij} = \frac{1}{2}\left((\nabla\theta)_i + (\nabla\theta)_i^T\right) \tag{2d}$$

$$\theta_i = \frac{1}{2}(\mathrm{curl}(\mathbf{u}))_i \tag{2e}$$

where μ, λ, l, r and θ are shear modulus, Lame constant, length scale parameter, displacement vector and rotation vector, respectively.

3 Governing equations

As shown in Fig. 1, the scanner is modeled by a moveable main plate suspended by two nanobeams over a fixed substrate electrode. In order to derive the equilibrium equations, it is required to compute the electrical and vdW forces (F_{elec} and F_{vdW}) and moments (M_{elec} and M_{vdW}) acting on the main plate.

3.1 Calculating of electrical force and moment

The electrical force of a differential element of the main plate can be written as [24]

$$\mathrm{d}F_{\mathrm{elec}} = \frac{\varepsilon b V^2}{2(D-\delta-r\sin(\theta))^2}\mathrm{d}r \tag{3}$$

where θ and δ are the rotation and deflection of main plate. Using (3), the total electrical force is obtained as:

$$\begin{aligned} F_{\mathrm{elec}} &= \int_{a_1}^{a_2} \mathrm{d}F_{\mathrm{elec}} \\ &= \frac{\varepsilon V^2 b}{2\sin(\theta)}\left(\frac{1}{D-\delta-a_2\sin(\theta)} - \frac{1}{D-\delta-a_1\sin(\theta)}\right) \end{aligned} \tag{4}$$

By applying $\sin(\theta)\approx\theta$, $\theta_{\max}=\frac{D}{a}$, $\Delta=\frac{\delta}{D}$, $\Theta=\frac{\theta}{\theta_{\max}}$, $\alpha=\frac{a_1}{a}$ and $\beta=\frac{a_2}{a}$ in Eq. (4), the electrical force can be simplified as:

$$F_{\mathrm{elec}} = \frac{\varepsilon V^2 b}{4\theta_{\max}\Theta D}\left\{\frac{1}{1-\Delta-\beta\Theta} - \frac{1}{1-\Delta-\alpha\Theta}\right\} \tag{5}$$

By using Eq. (3) the electric moment ($\mathrm{d}M_{\mathrm{elec}}$) can be explained as:

$$\mathrm{d}M_{\mathrm{elec}} = \frac{\varepsilon b V^2}{2(D-\delta-r\sin(\theta))^2} r\cos(\theta)\mathrm{d}r \tag{6}$$

Hence, the total electric moment is defined as:

$$\begin{aligned} M_{\mathrm{elec}} &= \int_{a_1}^{a_2}\mathrm{d}M_{\mathrm{elec}} = \frac{\varepsilon V^2 b\cos(\theta)}{2\sin^2\theta}\left\{\frac{D-\delta}{D-\delta-a_2\sin\theta}\right. \\ &\left. - \frac{D-\delta}{D-\delta-a_1\sin\theta} + \ln\left(\frac{D-\delta-a_2\sin\theta}{D-\delta-a_1\sin\theta}\right)\right\} \end{aligned} \tag{7}$$

Using dimensionless parameters and assuming $\sin(\theta)\approx\theta$ and $\cos(\theta)\approx 1$ Eq. (7) can be rewritten as

$$M_{\mathrm{elec}} = \frac{\varepsilon b V^2}{2\Theta^2\theta_{\max}^2}\left\{\frac{1-\Delta}{1-\Delta-\beta\Theta} - \frac{1-\Delta}{1-\Delta-\alpha\Theta} + \ln\left[\frac{1-\Delta-\beta\Theta}{1-\Delta-\alpha\Theta}\right]\right\} \tag{8}$$

3.2 Calculating of vdW force and moment

The vdW force of a differential element of the main plate can be written as [24]

$$\mathrm{d}F_{\mathrm{vdW}}^{L} = \frac{Ab}{6\pi(D-\delta-r\sin(\theta))^3}\mathrm{d}r \tag{9a}$$

$$\mathrm{d}F_{\mathrm{vdW}}^{R} = \frac{Ab}{6\pi(D-\delta+r\sin(\theta))^3}\mathrm{d}r \tag{9b}$$

By integrating Eq. (9), the total vdW force applied on main plate is obtained as:

$$\begin{aligned} F_{\mathrm{vdW}} &= \int_0^a (\mathrm{d}F_{\mathrm{vdW}}^{L} + \mathrm{d}F_{\mathrm{vdW}}^{R}) \\ &= \frac{Aab}{3\pi}\frac{D-\delta}{(D-\delta-a\sin(\theta))^2(D-\delta+a\sin(\theta))^2} \end{aligned} \tag{10}$$

Using dimensionless parameters, Eq. (10) can be rewritten as

$$F_{\mathrm{vdW}} = \frac{Aab}{3\pi D^3}\frac{1-\Delta}{(1-\Delta-\Theta)^2(1-\Delta+\Theta)^2} \tag{11}$$

By using Eq. (9), the vdW moment acting on a differential element ($\mathrm{d}M_{\mathrm{vdW}}$) can be obtained as:

$$\mathrm{d}M_{\mathrm{vdW}}^{L} = \frac{Ab}{6\pi(D-\delta-r\sin(\theta))^3} r\cos(\theta)\mathrm{d}r \tag{12}$$

$$\mathrm{d}M_{\mathrm{vdW}}^{R} = \frac{Ab}{6\pi(D-\delta+r\sin(\theta))^3} r\cos(\theta)\mathrm{d}r \tag{13}$$

Using (12) and (13), the total vdW moment is obtained as:

$$\begin{aligned} M_{\mathrm{vdW}} &= \int_0^a (\mathrm{d}M_{\mathrm{vdW}}^{L} - \mathrm{d}M_{\mathrm{vdW}}^{R}) \\ &= \frac{Aba^3\sin\theta\cos(\theta)}{3\pi(D-\delta-a\sin\theta)^2(D-\delta+a\sin\theta)^2} \end{aligned} \tag{14}$$

Using dimensionless parameters and assuming $\sin(\theta)\approx\theta$ and $\cos(\theta)\approx 1$ Eq. (14) can be rewritten as

$$M_{\mathrm{vdW}} = \frac{Ab\Theta}{3\pi D\theta_{\max}^2(1-\Delta-\Theta)^2(1-\Delta+\Theta)^2} \tag{15}$$

It should be noted that the beam have torsion and deflection simultaneously. In the following, the superposition principal is applied to derive the torsion and bending equilibrium of the rotational scanner.

3.3 Torsion equilibrium of the beam

Considering the same geometry for nanobeams, one can obtain the following equation for each nanobeam:

$$\frac{1}{2}(M_{\text{elec}} + M_{\text{vdW}}) - M_{\text{elas}} = 0 \tag{16}$$

In above relation, M_{elas} is the torsional elastic resistance moment of each nanobeam.

In order to calculate the elastic moment M_{elas} of the nanobeam based on couple stress theory, one can start with the Saint-Venant's approach. The elastic moment of the beam can be determined (see "Appendix 1") as the following:

$$M_{\text{elas}} = \frac{\mu\theta}{L}(J + J_{\text{c}}) \tag{17}$$

where J is the cross-section polar moment of inertia and J_{c} is the microstructure-dependent polar moment of inertia [35]:

$$J = \begin{cases} \dfrac{\pi t^4}{2} & \text{Circular} \\ \dfrac{tw^3}{3}\left[1 - \dfrac{192w}{\pi^5 t}\displaystyle\sum_{n=1}^{\infty}\frac{1}{(2n-1)^5}\tanh\left[\frac{(2n-1)\pi t}{2w}\right]\right] & \text{Rectangular} \end{cases} \tag{18}$$

$$J_{\text{c}} = \begin{cases} 3Al^2 & \text{Circular} \\ 3Al^2 + \dfrac{tw(w^2+t^2)}{12} + \displaystyle\iint_A \left(X\frac{\partial \Phi}{\partial Y} - Y\frac{\partial \Phi}{\partial X}\right)\mathrm{d}X\mathrm{d}Y & \text{Rectangular} \end{cases} \tag{19}$$

In the above relation, A, t and w are the area, thickness and width of the beam cross section, respectively. Furthermore, Φ is the warping function which is determined numerically (see "Appendix 1"). It should be noted that J_{c} is microstructure dependent, i.e., it is a function of the length scale parameter (l). For two typical cross-section geometries e.g., square and circular, the non-dimensional parameter J_{c}/J is plotted versus l/t in Fig. 2.

Now by substituting Eqs. (8), (15) and (17) into (16), we have:

$$\begin{aligned} &\frac{2\Theta\theta_{\max}\mu J\left(1+\frac{J_{\text{c}}}{J}\right)}{L} - \frac{\varepsilon b V^2}{2\Theta^2\theta_{\max}^2}\left\{\frac{1-\Delta}{1-\Delta-\beta\Theta} - \frac{1-\Delta}{1-\Delta-\alpha\Theta}\right. \\ &\left. + \ln\left[\frac{1-\Delta-\beta\Theta}{1-\Delta-\alpha\Theta}\right]\right\} \\ &- \frac{Ab\Theta}{3\pi D\theta_{\max}^2(1-\Delta-\Theta)^2(1-\Delta+\Theta)^2} = 0 \end{aligned} \tag{20}$$

Equation (20) expresses the torsion equilibrium of the nanobeams and relates rotation and deflection of the main plate to the external voltage as well as the microstructure parameter and vdW force.

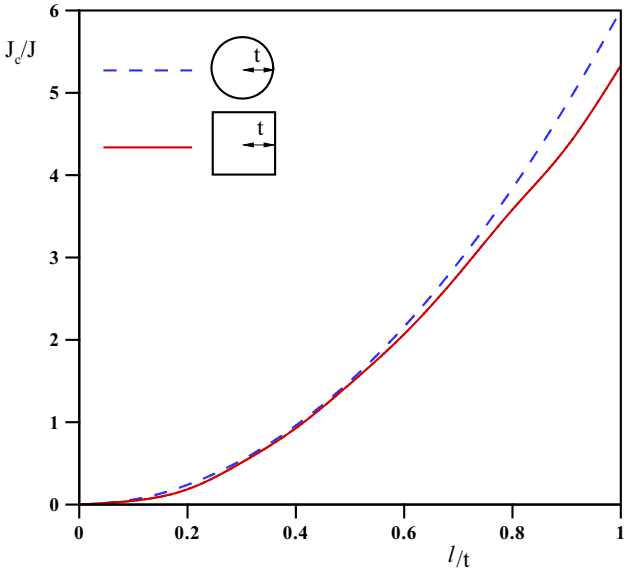

Fig. 2 Variation of J_{c}/J as a function of microstructure parameter (l/t) for different cross sections

3.4 Bending equilibrium of the beam

To find the bending equilibrium governing equation of the main plate, one can use an energy approach. By imposing the minimum energy for equilibrium, we obtain relations (21) for nanobeam (see "Appendix 2"):

$$\frac{1}{2}F_{\text{elec}} + \frac{1}{2}F_{\text{vdW}} - \frac{12.403(EI + \mu Al^2)}{L^3}\delta = 0 \tag{21}$$

Now by substituting Eqs. (5), (11) into (21) and using non-dimensional parameter, we have:

$$\begin{aligned} &\frac{\varepsilon V^2 b}{4\theta_{\max}\Theta D}\left\{\frac{1}{1-\Delta-\beta\Theta} - \frac{1}{1-\Delta-\alpha\Theta}\right\} \\ &+ \frac{Ab}{6\pi D^2\theta_{\max}}\frac{1-\Delta}{(1-\Delta-\Theta)^2(1-\Delta+\Theta)^2} \\ &- \frac{12.403(EI+\mu Al^2)D}{L^3}\Delta = 0 \end{aligned} \tag{22}$$

Equation (22) expresses the bending equilibrium of the nanobeams and relates the rotation and deflection of the main plate to the applied voltage, microstructure parameter and vdW attraction.

3.5 Solving the equilibrium equations

To determine the instability parameters of the scanner, Eqs. (20) and (22) can be rearranged in the new following forms:

$$\Xi_1(\Theta,\Delta)=\overline{V}=\left\{\frac{\left(1+\frac{J_c}{J}\right)\Theta^4-\frac{\xi\Theta^3}{(1-\Delta-\Theta)^2(1-\Delta+\Theta)^2}}{\frac{\Theta(1-\Delta)}{1-\Delta-\beta\Theta}-\frac{\Theta(1-\Delta)}{1-\Delta-\alpha\Theta}+\Theta\ln\left(\frac{1-\Delta-\beta\Theta}{1-\Delta-\alpha\Theta}\right)}\right\}^{\frac{1}{2}} \tag{23}$$

$$\Xi_2(\Theta,\Delta)=\Xi_1(\Theta,\Delta)-\left\{\frac{K^2\left(1+\frac{6}{1+\upsilon}\left(\frac{l}{t}\right)^2\right)\Delta\Theta^2-\frac{\xi\Theta(1-\Delta)}{(1-\Delta-\Theta)^2(1-\Delta+\Theta)^2}}{\frac{\Theta}{1-\Delta-\beta\Theta}-\frac{\Theta}{1-\Delta-\alpha\Theta}}\right\}^{\frac{1}{2}}=0 \tag{24}$$

where

$$\xi=\frac{\mathrm{AbL}}{6\pi D\theta_{\max}^3\mu J} \tag{25a}$$

$$\overline{\mathrm{V}}^2=\frac{\varepsilon \mathrm{V}^2\mathrm{bL}}{4\mu J\theta_{\max}^3} \tag{25b}$$

$$K=\frac{\mathrm{D}}{\theta_{\max}\mathrm{L}}\sqrt{\frac{12.403\mathrm{EI}}{\mu\mathrm{J}}} \tag{25c}$$

The parameter K shows the ratio of bending stiffness to torsion stiffness of the nanobeam. The torsion mode is dominant in the case of large K, while the bending mode is dominant for low K values.

Equations (23) and (24) are solved to determine the rotation (Θ) and deflection (Δ) of the scanner for any applied voltage difference ($\bar{V}$). According to the implicit function theorem [6], the pull-in point should be satisfied the following condition:

$$\begin{vmatrix}\frac{\partial\Xi_1}{\partial\Theta}(\Theta_{\mathrm{PI}},\Delta_{\mathrm{PI}}) & \frac{\partial\Xi_1}{\partial\Delta}(\Theta_{\mathrm{PI}},\Delta_{\mathrm{PI}})\\ \frac{\partial\ \Xi_2}{\partial\Theta}(\Theta_{\mathrm{PI}},\Delta_{\mathrm{PI}}) & \frac{\partial\ \Xi_2}{\partial\Delta}(\Theta_{\mathrm{PI}},\Delta_{\mathrm{PI}})\end{vmatrix}=0,\quad \Xi_2(\Theta_{\mathrm{PI}},\Delta_{\mathrm{PI}})=0 \tag{26}$$

From relation (26), the instability parameters of the scanner which are defined as Θ, Δ at the pull-in point (Θ_{PI} and Δ_{PI}) are determined as a function of the geometrical parameters (α and β), coupling parameter (K) and the length scale parameters (l). Finally, by substituting the obtained Θ_{PI} and Δ_{PI} in Eq. (23), $\bar{V}$ at the pull-in point ($\bar{V}_{PI}$) is determined.

4 Result and discussion

4.1 Bending/torsion coupled instability

Influence of coupling ratio (K) geometrical parameter (β) on the pull-in behavior of typical microscanner is shown in Figs. 3, 4 and 5. As seen, the pull-in behavior depends on the value of the coupling parameter (K). For systems with $K \geq 15$, the instability angle is close to the results of pure torsion model ($K = \infty$). Interestingly, if both bending and torsion stiffness are considerable, an increase–decrease trend can be observed in Θ_{PI}–β curves. It is due to the conquering of the bending pull-in mode over the torsion mode. Moreover, the instability voltage determined by the 2-DOF model is lower than that of the 1-DOF model value.

Figure 6 shows the influence of the aspect ratio (L/t) on the pull-in angle and pull-in deflection. This figure reveals

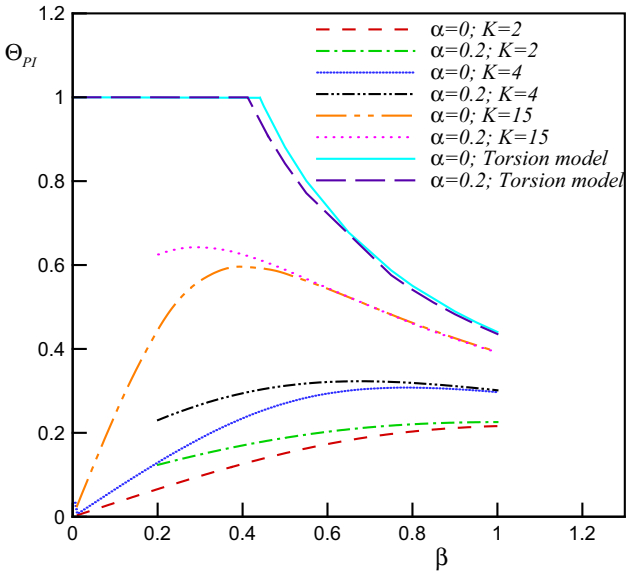

Fig. 3 Impact of geometry parameter (β) and coupling ration (K) on the pull-in angle

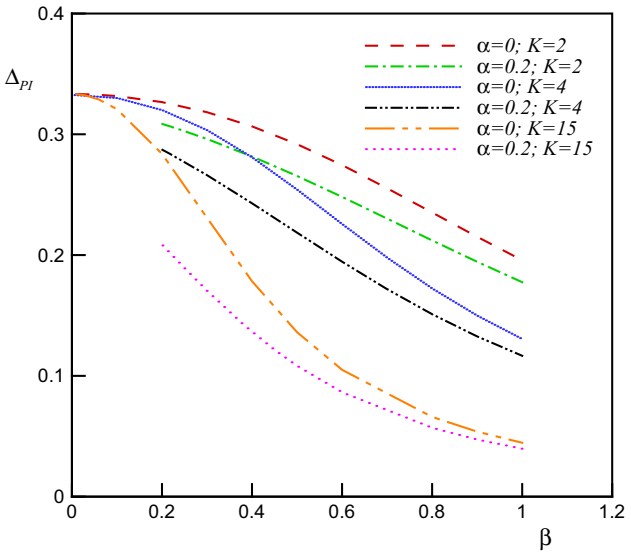

Fig. 4 Impact of geometry parameter (β) and coupling ration (K) on the pull-in displacement

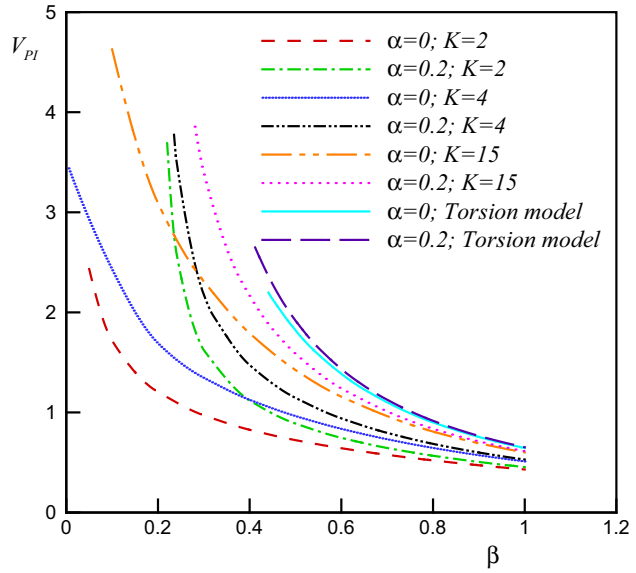

Fig. 5 Impact of geometry parameter (β) and coupling ration (K) on the pull-in voltage

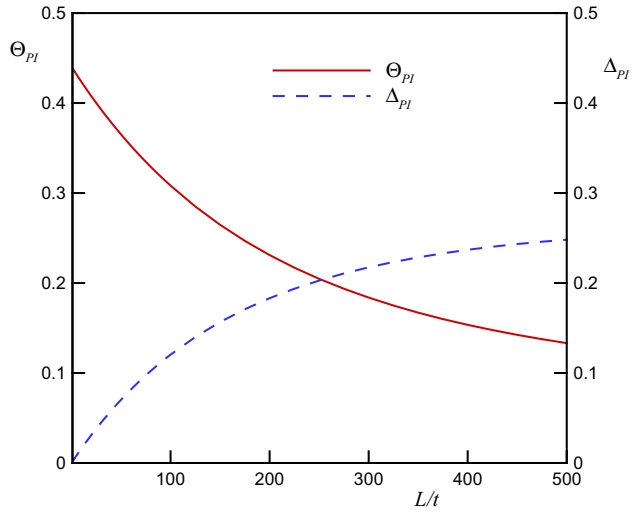

Fig. 6 Impact of ratio (L/t) on the pull-in parameters

that by increasing the aspect ratio, the pull-in deflection increases while the pull-in angle decreases. It is clear from Fig. 6 that for $L/t < 20$ the pull-in deflection is less than 0.03 % and the difference between the 2-DOF and 1-DOF model is less than 7 %, but for $L/t > 20$ the difference between 1-DOF and 2-DOF modes is dominant.

4.2 Microstructure effect

Figures 7, 8 and 9 illustrate the impact of length scale parameter on the instability behavior of the typical scanner. As seen, microstructure effect enhances the instability threshold of the nanoscanner. The microstructure dependency increases the pull-in voltage and pull-in deflection of

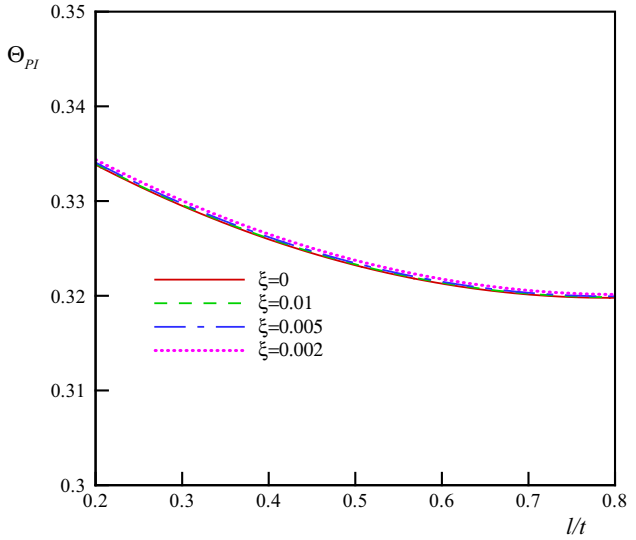

Fig. 7 Influence of microstructure and vdW force on the pull-in angle ($\alpha = 0.06$ and $\beta = 0.84$ and $K = 5$)

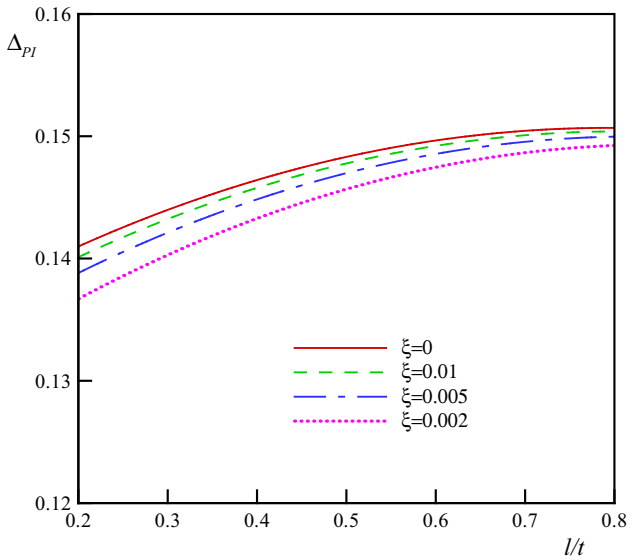

Fig. 8 Influence of microstructure and vdW force on the pull-in displacement (l/t) ($\alpha = 0.06$ and $\beta = 0.84$ and $K = 5$)

the scanners and reduces the pull-in angle. The pull-in voltage calculated by the microstructure-dependent model is higher than that determined by the classical theory. In addition, this stiffening trend is more important for larger l/t values. Figures 7, 8 and 9 reveal that when the thickness of the torsional beam is in the order of the material length scale parameter, classic models might not be precise enough for determining the pull-in parameters of miniature scanners fabricated from microstructure-dependent materials.

The effects of microstructure as well as vdW force on the instability of a typical scanner are demonstrated in

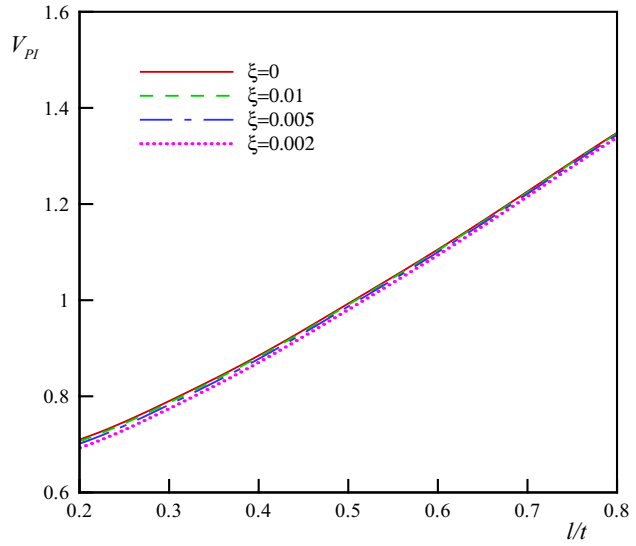

Fig. 9 Influence of microstructure and vdW force on the pull-in voltage ($\alpha = 0.06$ and $\beta = 0.84$ and $K = 5$)

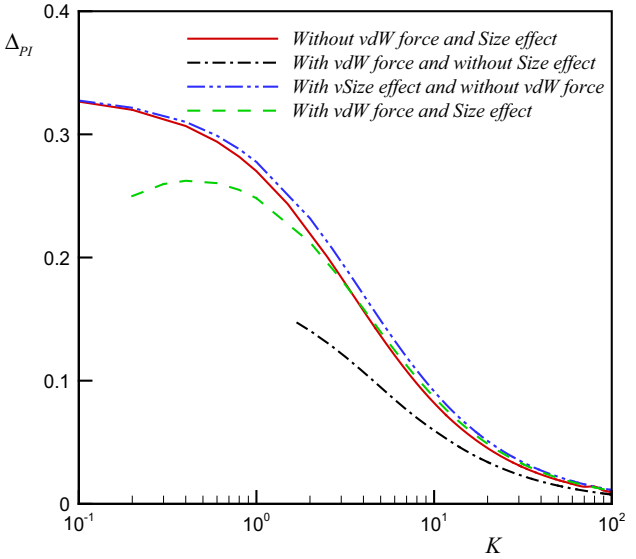

Fig. 11 Variation of pull-in displacement versus K parameter: impact of microstructure and vdW force ($\alpha = 0.06$ and $\beta = 0.84$)

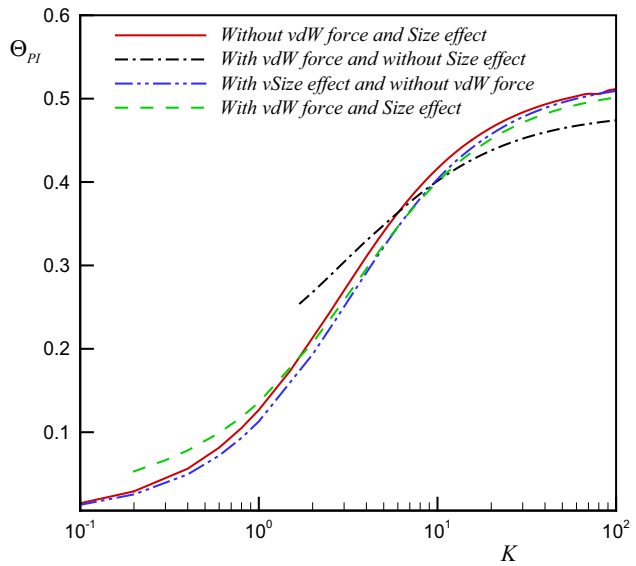

Fig. 10 Variation of pull-in angle versus K parameter: impact of microstructure and vdW force ($\alpha = 0.06$ and $\beta = 0.84$)

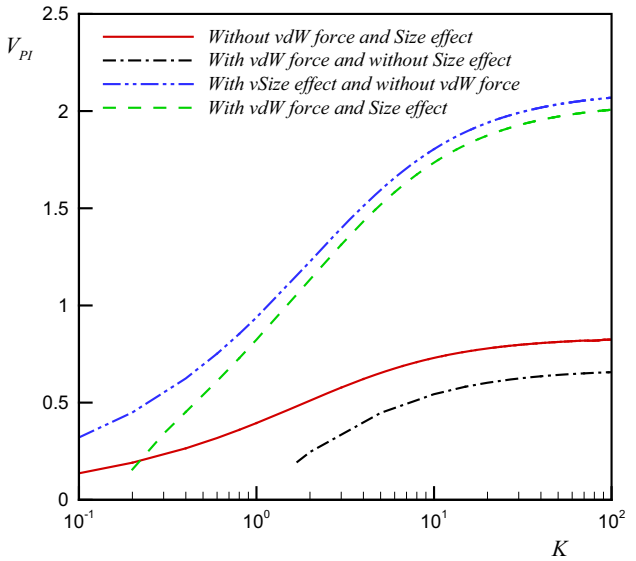

Fig. 12 Variation of pull-in voltage versus K parameter: impact of microstructure and vdW force ($\alpha = 0.06$ and $\beta = 0.84$)

Figs. 10, 11 and 12 where the variation of the instability parameters is presented versus the coupling ratio (K). As seen, the vdW force has a softening effect and reduces the pull-in voltage. While microstructure effect increases the stability of the system, vdW force reduces the instability threshold of the system.

4.3 Validation

Figure 13 compares the pull-in voltage predicted by the presented model with those obtained experimentally by Zhan et al. [21]. As seen, while the classical model ($l = 0$) cannot predict the pull-in voltage accurately, the results of presented size-dependent model are very close to experimental data.

Table 1 compares the pull-in parameters depict by presented model and the experimental results obtained by Huang et al. [22]. This table implies that the instability parameters determined by the proposed model are in good agreement with those of experimental. In particular, the pull-in parameters determined by the present model are closer to the experimental values than the 1-DOF torsion model. Figure 6 and Table 1 demonstrate that the presented model is in better agreement with experiments in

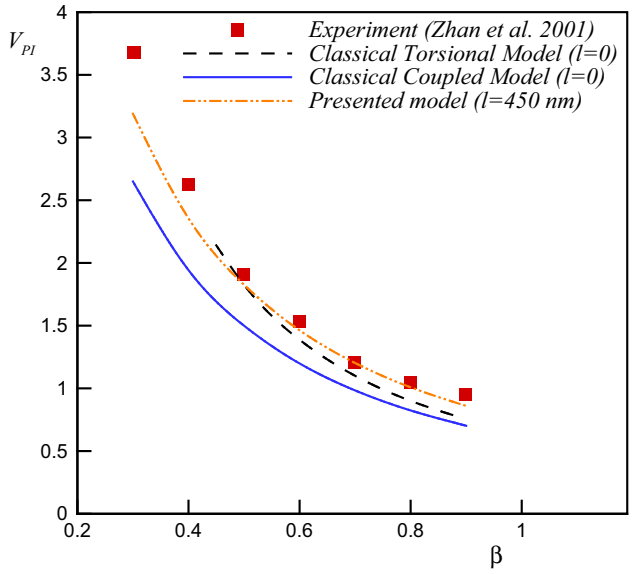

Fig. 13 Comparison the pull-in voltage calculate by theoretical models with experimental results

comparison with the 1-DOF torsional and classical 2-DOF models. Indeed, both of these models present uniform trends, i.e., softening (for 2-DOF model) or hardening (for 1-DOF models). However, the presented model is able to predict both hardening and softening behavior depending on the geometry and constitutive material.

5 Conclusions

A microstructure-dependent model has been presented to investigate the coupled torsion/bending pull-in instability of nanoscanner in the presence of vdW attraction. It is found that the pull-in voltage decreases with decreasing coupling ratio. It is found that neglecting the microstructure effect may cause major error in simulation of the system. Increasing the microstructure effect causes a hardening effect, i.e., decreases the instability voltage. Impact of microstructure on instability voltage of the nanoscanner depends on coupling ratio and the conquering bending mode over torsion mode. This effect is more highlighted for higher values of coupling ratio.

Appendix 1

In order to calculate the elastic moment M_{elas} of the nanobeam based on MCST, one can start with the Saint-Venant's approach and assume the displacement field as [36]:

$$\begin{aligned} u_1 &= -\Omega YZ \\ u_2 &= -\Omega XZ \\ u_3 &= \Omega \Phi(X,Y) \end{aligned} \tag{27}$$

where u_1, u_2 and u_3 are the displacement along the X, Y and Z direction, respectively. Furthermore, Ω is the angle of twist per unit length along the beam, and the function $\Phi(X, Y)$ is the warping function depending on X and Y only. For more details about warping effect, see [37, 38].

The governing equation of the torsional bar based on MCST can be obtained as (see [35, 39] for details):

$$\frac{l^2}{4}\frac{\partial^4 \Phi}{\partial X^4} + \frac{l^2}{4}\frac{\partial^4 \Phi}{\partial Y^4} + \frac{l^2}{2}\frac{\partial^4 \Phi}{\partial X^2 \partial Y^2} - \frac{\partial^2 \Phi}{\partial X^2} - \frac{\partial^2 \Phi}{\partial Y^2} = 0 \tag{28}$$

with the boundary conditions of:

$$\begin{aligned} &\frac{\partial \Phi}{\partial n} - \frac{l^2}{4}\frac{\partial^3 \Phi}{\partial n^3} - \frac{l^2}{2}\frac{\partial^3 \Phi}{\partial n \partial s^2} + \frac{l^2}{2}\frac{\partial}{\partial s}\left(\frac{1}{\rho}\frac{\partial \Phi}{\partial s}\right) - n_X Y + n_Y X = 0 \\ &\frac{\partial^2 \Phi}{\partial n^2} - \frac{\partial^2 \Phi}{\partial s^2} - \frac{2}{\rho}\frac{\partial \Phi}{\partial n} = 0 \end{aligned} \tag{29}$$

In the above relations, ρ, $n(n_x,n_y)$ and $s(-n_y,n_x)$ are the curvature, the unit vector normal to the boundary and the unit tangent to the boundary, respectively [35, 39].

Appendix 2

It should be noted that for thick and short beam (i.e., $L/t < 20$) the Timoshenko beam model should be used [26]. However, the difference between the 1-DOF and 2-DOF results is negligible for $L/t < 20$, and simple 1-DOF model can be used (see Fig. 6). Hence, the Euler–Bernoulli beam theory is employed in this work. Based on the Euler–Bernoulli beam theory, components of the displacement vector for bending beam are expressed as [36]

Table 1 Comparison between the pull-in parameters obtained by the experiment and those of different theories ($K = 3.243$, $\bar{A} = 4 \times 10^{-19}$ J)

Model	V_{PI} (V)	Error* (%)	Θ_{PI}	Error* (%)	Δ_{PI}	Error* (%)
Experiment [21]	17.4	–	0.4198	–	0.0778	–
1-DOF torsion model [21]	20.1	15.5	0.5236	24.7	–	–
Presented model ($l = 150$ nm)	18.17	4.4	0.4270	1.7	0.0752	3.34
Presented model ($l = 0$)	17.68	1.6	0.4270	0.9	0.0778	0

* Relative error with experiment

$$\begin{aligned} u_1(Z) &= 0 \\ u_2(Z) &= v(Z) \\ u_3(Z) &= -Y\frac{\partial v(Z)}{\partial Z} \end{aligned} \tag{30}$$

where u_1, u_2 and u_3 are the displacement along the X, Y and Z direction, respectively.

By substituting this displacement field in Eq. (2) and substituting the results in Eq. (1), the bending elastic energy, U_b, can be determined as:

$$U_b = \frac{1}{2}\int_0^L \left(EI + \mu A l^2\right)\left(\frac{d^2 v}{dZ^2}\right)^2 dz \tag{31}$$

The work by the external forces can be obtained as:

$$w_e \int_0^{v=v(L)} \left(\frac{1}{2}[F_{vdW} + F_{elec}]\right) dw \tag{32}$$

As a trial solution for deflection of the nanobeam, the first mode shape which satisfies the boundary conditions can be selected as:

$$\begin{aligned} V(Z) = \frac{\delta}{1.588}&[\cosh(2.365Z) - \cos(2.365Z) \\ &- V0.9825(\sinh(2.365Z) - \sin(2.365Z)) \end{aligned} \tag{33}$$

By substituting Eq. (33) in Eq. (31), the total energy of system, Π, can be written as:

$$\begin{aligned} \Pi = \Pi &= U_b - W_e \\ &= \frac{6.2015(EI + \mu A l^2)}{L^3}\delta^2 - \frac{1}{2}\int_0^{\delta} (F_{vdW} + F_{elec}) dv \end{aligned} \tag{34}$$

By imposing the minimum energy for equilibrium, i.e., $\frac{\partial \Pi}{\partial \delta} = 0$, we obtain relations (24) for nanobeam.

References

1. X.M. Zhang, F.S. Chau, C. Quan, Y.L. Lam, A.Q. Liu, Sensor Actuators A **90**, 73 (2001)
2. W.H. Lin, Y.P. Zhao, J. Phys. D **40**, 1649 (2007)
3. C. Venkatesh, N. Bhat, **8**(1), 129 (2008)
4. C. Venkatesh, S. Pati, N. Bhat, R. Pratap, Sensors Actuators A **121**(2), 480 (2005)
5. C. Venkatesh, N. Bhat, K.J. Vinoy, S. Grandhi, J. Micro-Nanolith. Mem. **11**(1), 013006 (2012)
6. O. Degani, Y. Nemirovsky, J. Microelectromech. Syst. **11**, 20 (2002)
7. H. Moeenfard, A. Darvishian, M.T. Ahmaidan, J. Mech. Sci. Technol. **26**, 537 (2012)
8. J.E. Ford, V.A. Aksyuk, D.J. Bishop, J.A. Walker, J. Lightwave Technol. **17**, 904 (1999)
9. J.G. Guo, Y.P. Zhao, J. Microelectromech. Syst. **13**(6), 1027 (2004)
10. J.G. Guo, Y.P. Zhao, Int. J. Solids Struct. **43**, 675 (2006)
11. F. Khatami, G. Rezazadeh, Microsyst. Technol. **15**, 535 (2009)
12. H.M. Sedighi, K.H. Shirazi, Acta Mech. Solida Sin. **28**(1), 91 (2015)
13. M.I. Younis, F. Alsaleem, D. Jordy, Int. J. Nonlin. Mech. **42**(4), 643 (2007)
14. M. Taghizadeh, H. Mobki, Arch. Mech. **66**(2), 95 (2014)
15. J.P. Zhao, H.L. Chen, J.M. Huang, A.Q. Liu, Sensors Actuators A **120**, 199 (2005)
16. H. Moeenfard, M.T. Ahmadian, Optik **124**(12), 1278 (2013)
17. Z.X. Xiao, X.T. Wu, W.Y. Peng, K.R. Farmer, J. Microelectromech. Syst. **10**, 561 (2001)
18. Y. Nemirovsky, O. Degani, J. Microelectromech. Syst. **10**, 601 (2001)
19. O. Degani, E. Socher, A. Lipson, T. Leitner, D.J. Setter, S. Kaldor, Y.J. Nemirovsky, Microelectromech. Syst. **7**(4), 373 (1998)
20. H. Moeenfard, A. Darvishian, H. Zohoor, M.T. Ahmadian, J. Mech. Eng. Sci. **226**(9), 2361–2372 (2012)
21. O.B. Degani, Y. Nemirovisky, Sensor Actuators A **97–98**, 569 (2001)
22. J.M. Huang, A.Q. Liu, Z.L. Deng, Q.X. Zhang, J. Ahn, A. Asundi, Sensor Actuators A **115**(1), 159 (2004)
23. G. Rezazadeh, F. Khatami, A. Tahmasebi, Microsyst. Tech. **13**, 715 (2007)
24. Y. Tadi Beni, A. Koochi, A.S. Kazemi, M. Abadyan, Can. J. Phys. **90**(10), 963 (2012)
25. Y. Tadi, Iran J. Sci. B **36**(M1), 41 (2012)
26. N.H. Nguyen, M.Y. Lee, J.S. Kim, D.Y. Lee, Shock Vibration **2015**, 672831 (2015)
27. N.A. Fleck, G.M. Muller, M.F. Ashby, J.W. Hutchinson, Acta Metall. Mater. **42**(2), 475 (1994)
28. B. Akgöz, Ö. Civalek, Curr. Appl. Phys. **11**, 1133–1138 (2011)
29. B. Akgoz, O. Civalek, Int. J. Eng. Sci. **49**(11), 1268 (2011)
30. J. Abdi, A. Koochi, A.S. Kazemi, M. Abadyan, Smart Mater. Struct. **20**(5), 055011 (2011)
31. Y. Tadi Beni, A. Koochi, M. Abadyan, Physica E **43**, 979 (2011)
32. J.G. Guo, Y.P. Zhao, Int. J. Solids Struct. **43**, 675 (2006)
33. Y. Tadi Beni, M. Abadyan, Int. J. Mod. Phys. B **27**(18), 1350083 (2013)
34. F. Yang, A.C.M. Chong, D.C.C. Lam, P. Tong, Int. J. Solids Struct. **39**(10), 2731 (2002)
35. P. Tong, F. Yang, D.C.C. Lam, J. Wang, Key Eng. Mater. **261–263**, 11–22 (2004)
36. C.L. Dym, I.H. Shames, *Solid Mechanics: A Variational Approach* (Railway Publishing House, Beijing, 1984)
37. N.H. Nguyen, B.D. Lim, D.Y. Lee, Int. J. Precision Eng. Manufact. **16**(4), 749–754 (2015)
38. N.H. Nguyen, B.D. Lim, D.Y. Lee, Struct. Eng. Mech. **54**(1), 189–198 (2015)
39. G.C. Tsiatas, J.T. Katsikadelis, Eur. J. Mech. A-Solid **30**, 741–747 (2011)